Probing the Location of Hot Spots by Surface-Enhanced Raman Spectroscopy: Toward Uniform Substrates

Xiang Wang,[†] Maohua Li,[†] Lingyan Meng,[‡] Kaiqiang Lin,[†] Jiamin Feng,[†] Tengxiang Huang,[†] Zhilin Yang,[‡,*] and Bin Ren[†,*]

[†]State Key Laboratory of Physical Chemistry of Solid Surfaces, MOE Key Laboratory of Spectrochemical Analysis and Instrumentation, Collaborative Innovation Center of Chemistry for Energy Materials, and Department of Chemistry, College of Chemistry and Chemical Engineering, Xiamen University, Xiamen 361005, China, and [‡]Department of Physics, School of Physics and Mechanical Engineering, Xiamen University, Xiamen 361005, China

ABSTRACT Wide applications of surface plasmon resonance rely on the in-depth understanding of the near-field distribution over a metallic nanostructure. However, precisely locating the strongest electric field in a metallic nanostructure still remains a great challenge in experiments because the field strength decays exponentially from the surface. Here, we demonstrate that the hot spot position for gold nanoparticles over a metal film can be precisely located using surface-enhanced Raman spectroscopy (SERS) by rationally choosing the probe molecules and excitation wavelengths. The finite difference time domain simulation verifies the experimental results and further reveals that the enhancement for the above system is sensitive to the distance between nanoparticles and the metal film but insensitive to the distance of nanoparticles. On the basis of this finding, we propose and demonstrate an approach of using a nanoparticles-on-metal film substrate as a uniform SERS substrate. This work provides a convenient way to probe the location of strong near-field enhancement with SERS and will have important implications in both surface analysis and surface plasmonics.

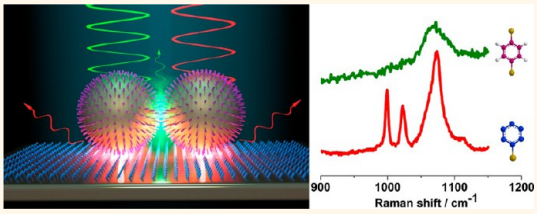

KEYWORDS: surface plasmon resonance · nanoparticle · gold film · near-field distribution · hot spot · uniform SERS substrate

Surface plasmon resonance (SPR) of metals, due to the collective oscillation of free electrons, has attracted tremendous interest in many fascinating fields, such as nanosensors,[1] nano-optics,[2,3] nanoelectronics,[4] biology,[5] and photovoltaics.[6] Metal nanostructures exhibit bright colors due to their strong SPR effects in the visible and near-infrared region. In fact, the SPR leads to a strongly enhanced electric field on the surfaces of metal nanostructures, resulting in a significantly enhanced efficiency of a range of optical processes on surfaces, including Raman,[7] fluorescence,[8] and second-harmonic effects.[9] Surface-enhanced Raman spectroscopy (SERS) is one of the most important spectroscopies inherently originated from the SPR of metal nanostructures.[10−12] It has been widely applied in chemical, physical, material, and biological analysis[13−16] since it is capable of providing fingerprint information of probe molecules at the single-molecule level.[17−19]

In practice, two kinds of substrates have been widely used for SERS detection: metal nanoparticle colloids and solid SERS substrates.[20−22] The former are usually induced to form nanoparticle aggregates to generate effective coupling and strong Raman signals. The latter, which involve fabrication of nanostructures with SERS activity or assembly of nanoparticles on a solid support, are more commonly used in SERS measurement owing to the ease of operation. Glass and silicon are two of the most widely used solid supports. The presence of a dielectric material around the nanoparticles will lead to an obvious shift of the SPR peaks of metal nanoparticles, but will not result in an obvious change of the near-field distribution of the electric field (Scheme 1a).[23] However, if a metallic solid support is used, a much stronger SERS signal will be observed than

* Address correspondence to (Z. L. Yang) zlyang@xmu.edu.cn; (B. Ren) bren@xmu.edu.cn.

Received for review September 30, 2013 and accepted December 16, 2013.

Published online December 16, 2013
10.1021/nn405073h

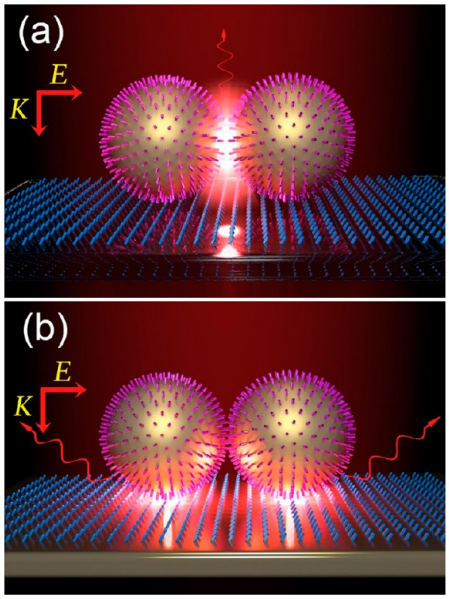

Scheme 1. (a) Metal nanoparticles dispersed on a dielectric support. The SERS signal is contributed by the molecules adsorbed on nanoparticles. (b) Metal nanoparticles dispersed on a gold support. The SERS signal is contributed by the molecules adsorbed on the smooth gold surface.

in the case of dielectric supports. In particular, the strong Raman signals of a monolayer of molecules adsorbed on smooth metal surfaces (including both gold and platinum) with gold and silver nanoparticles were observed[24−27] even when illuminating perpendicularly with the electric field vector polarized parallel to the surface (Scheme 1b). This means that the signal comes from the gap region between the nanoparticle and the substrate instead of from the gap between nanoparticles. This phenomenon appears to be contradictory to the common understanding that the strongest coupling should occur in the gap between nanoparticles when the laser is polarized parallel to the central axis of the two particles.[28−30] On the other hand, many works[31−35] have shown that the coupling between a metal nanoparticle and the gold substrate can only be efficiently induced by maximizing the component of light polarized perpendicularly to the metal surface. Obviously, the introduction of the metallic substrate completely changes the local distribution of the electric field.

This phenomenon points to an important issue in surface plasmonics: how to precisely predict and measure the distribution of the near-field electric field when there are more than one SPR coupling mode and more than one enhanced near-field position in a nanostructure. Clarifying this issue will be helpful in extracting meaningful information for further applications in plasmon-enhanced spectroscopy and plasmonic waveguides. However, it is well known that the SPR-induced electromagnetic field is tightly confined near the surface. The enhancement decays exponentially with the increase of the distance to the surface and extends only a few to tens of nanometers away from the surface, which makes the measurement of the near-field distribution a great challenge. The traditional optical techniques, such as dark-field microscopy and UV−vis spectroscopy, can provide only the SPR-induced far-field scattering or extinction information, which is insufficient to correlate the far-field information with the near-field distribution without the help of the theoretical calculation. Scanning near-field optical microscopy (SNOM) is capable of providing the optical information at a spatial resolution breaking the diffraction limit. However, it is still a challenge for SNOM to obtain the three-dimensional information to reflect the local distribution of the electric field. The most important issue is that the SNOM probe itself may change the near-field distribution of metal nanostructures.[36,37] Therefore, a method to correctly reflect the near-field distribution and enhancement is highly desired.

SERS is a phenomenon that employs the SPR-induced optical field enhancement to increase the Raman signals of adsorbed molecules on metal surfaces. It has been revealed that 98% of the SERS signals are contributed by 2% of the molecules adsorbed at strongly enhanced positions on the probe nanostructures (so-called hot spots).[38,39] Therefore, only the locations at metal nanostructures with a strong near-field enhancement (hot spot) will dominantly contribute to the obtained Raman signals. According to this correlation, the SERS signal of a probe molecule is capable of detecting the location with a strong near-field enhancement of metal nanostructures.[40] More recently, the super-resolution optical method has been used to image the single-molecule SERS hot spot.[41,42]

Therefore, in the present work, we chose a coupling system consisting of a gold nanoparticle dimer and a gold film to simulate the experimental system and to calculate the wavelength-dependent near-field distribution by the finite difference time domain (FDTD) method. Experimentally, we dispersed a homogeneous monolayer of gold nanoparticles over a gold film. We controlled the adsorption of two types of probe molecules with distinct Raman spectral features but similar Raman cross section at different positions of the nanoparticle dimer−film system, such as the nanoparticle surface or the gold film surface. Then we used different excitation wavelengths to selectively excite the desired species. The feasibility of using SERS to probe the near-field distribution has important implications in both SERS and surface plasmonics. Furthermore, we demonstrated a uniform SERS substrate that exhibits much more homogeneous signals than traditional substrates involving nanoparticles dispersed.

RESULTS AND DISCUSSION

Figure 1 presents the extinction spectra of the dimer−film coupling system in the visible and near-infrared region as well as the near-field distribution at

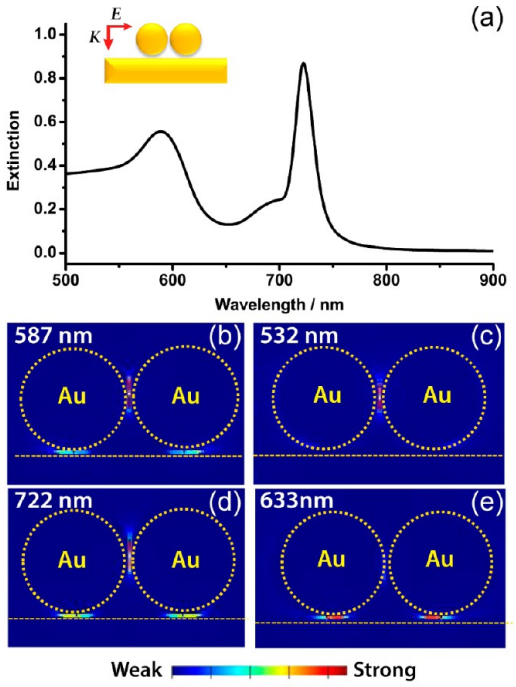

Figure 1. (a) Calculated extinction spectra for the gold dimer–film coupling system with FDTD. The model shown in the inset indicates the direction and polarization of the incident laser. (b, c, d, e) Images of the near-field distribution of the electric field under the excitation wavelengths of 587, 532, 722, and 633 nm, respectively. Images (b)–(e) are presented in different scales.

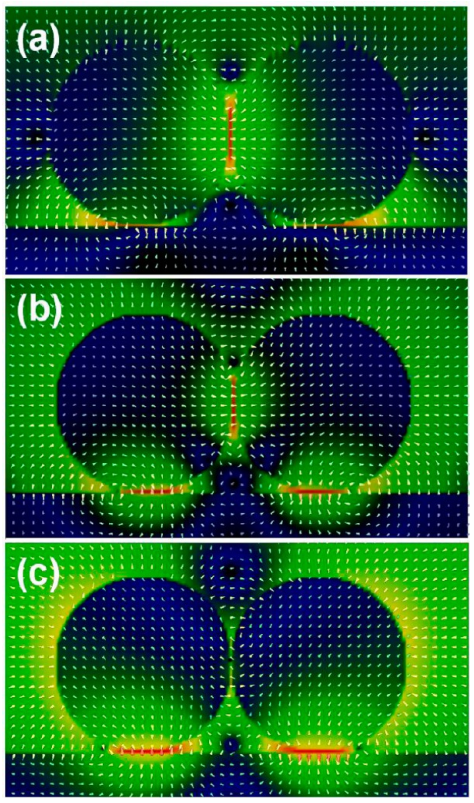

Figure 2. Snapshots of the dipole direction and distribution inside and outside metals during the interaction of light with the gold dimer–film system with FDTD simulation. (a) Initial state that the light interacts with gold nanoparticles. (b) Transient state showing a competition between the coupling mode between nanoparticles and the coupling mode between nanoparticles and the gold film. (c) Steady state where the electric field is confined in the gap between nanoparticles and the gold film.

four characteristic wavelengths, including the two extinction maxima and the two experimental laser wavelengths. The peak at 587 nm can be assigned to the LSPR mode of the individual gold nanoparticle, showing a relatively low near-field enhancement of about 8×10^3 (Figure 1b). The intense peak at 722 nm is a result of the effective coupling of the SPR mode of two gold nanoparticles, showing a strong near-field enhancement of about 1.2×10^5 (Figure 1d). To correlate the simulation with experiments, we examined the near-field distribution of the gold dimer–film coupling system at 532 and 633 nm, which are the two most common laser lines in SERS experiments. It was interesting to observe that the near-field enhancement is totally localized at the gap between two gold nanoparticles and the gap between nanoparticles and the gold film excited at 532 and 633 nm, respectively. The field enhancements outside these two regions are negligible as compared with their respective maxima. This phenomenon is much different from the case where a single gold nanoparticle sits 1 nm above the gold film (Supporting Information S1).

To understand the wavelength dependence of the distribution of near-field enhancement, we take some transient snapshots of the dipole direction and distribution inside and outside the metals during the interaction of light (633 nm) with the gold dimer–film system. As shown in Figure 2a, at the initial stage of interaction with light, the free electrons undergo oscillation along the axis of two nanoparticles parallel to the surface. A large amount of free electrons are involved in the oscillation in this dipole direction, resulting in a strong electric field in the gap of the two nanoparticles and leading to a partial positive field at the bottom of the nanoparticles. Therefore, the free electrons in the gold film reservoir are induced to gather under the nanoparticles as a result of the electrostatic effect. Then, the redistribution of electrons/dipoles will occur. Figure 2b shows such a redistribution as a result of the competition between the SPR coupling between nanoparticles and the coupling between nanoparticles and the gold film. In this case, the electrons are confined at two positions, with similar surface charge density. However, the distribution of electrons/dipoles in a specific metal structure finally has to reach a state in phase with the wavelength of excitation light. Figure 2c shows the distribution in the steady state of the gold dimer–film system excited at 633 nm. The free electrons gather at the bottom of nanoparticles to form a relatively strong near-field coupling with the gold film. However, due to the

competition among different SPR modes, the near-field intensity enhancement factor excited at 633 nm is decreased to only around 2.8×10^3, which is much weaker than that excited at 722 nm (1.2×10^5).

In the case of 532 nm excitation, few free electrons can gather in the dipole direction of the nanoparticle parallel to surface. As a result, there are no obvious changes in the surface charges at the bottom of the nanoparticles, which is insufficient to induce the gathering of free charges in the gold film. Therefore, the gold dimer–film system shows very weak coupling in the gap between the nanoparticles and the gold film. Furthermore, the near-field enhancement is also weak in the gap between nanoparticles, with a near-field enhancement factor of around 80.

Though the near-field enhancement excited at 722 nm is intense, the distribution of electric field has extended over the nanoparticles and the film. While the enhancement excited at 532 and 633 nm is relatively weak, the spatial distributions are explicit; that is, the hot spot is located at the gap between the gold nanoparticles exited at 532 nm and at the gap between the nanoparticles and the gold film exited at 633 nm. If we use two different kinds of molecules to occupy different positions, we may be able to probe the locations of different hot spots and the near-field distribution experimentally. In fact, the location of different hot spots presents the different excited modes with different surface charge distributions. A scheme of such a concept is given in the left panel of Figure 3a and b. We have used thiophenol (TP) and 1,4-benzenedithiol (BDT) as the two SERS probe molecules, because they have similar Raman cross sections and adsorption behaviors on the gold surface, which is highly important for the present experiment. We show the SERS spectra of TP and BDT molecules adsorbed on SERS-active gold nanoparticle substrates in the Supporting Information (Figure S5). BDT shows peaks at 1008, 1064, and 1178 cm^{-1}, and the TP shows peaks at 998, 1022, and 1072 cm^{-1}. Most of the Raman peaks of the two molecules overlap heavily because of their similar molecular structures. However, the peaks at around 1000 cm^{-1} show quite different features. The peak at 998 cm^{-1} is distinctly present in TP and is absent in BDT, so it can be used to distinguish TP and BDT molecules. BDT shows a much broader peak than TP at around 1064 cm^{-1}, and the peak can be considered the characteristic peak of BDT. Therefore, we can use these two peaks to demonstrate the different near-field distribution.

To perform the experiments, the TP molecules were adsorbed on a clean gold film first. Then a monolayer film of gold nanoparticles of 55 nm diameter was transferred on the gold film with TP molecules after rinsing with ethanol. Afterward, the sample was immersed in an ethanol solution containing BDT molecules (see Methods section). The scheme is shown in Figure 3a. In this configuration, we obtained the sample with TP molecules adsorbed in the gap between the nanoparticles and the gold film and BDT molecules adsorbed in the gap between the nanoparticles. The configuration can be reversed if we change the adsorption sequence of TP and BDT molecules.

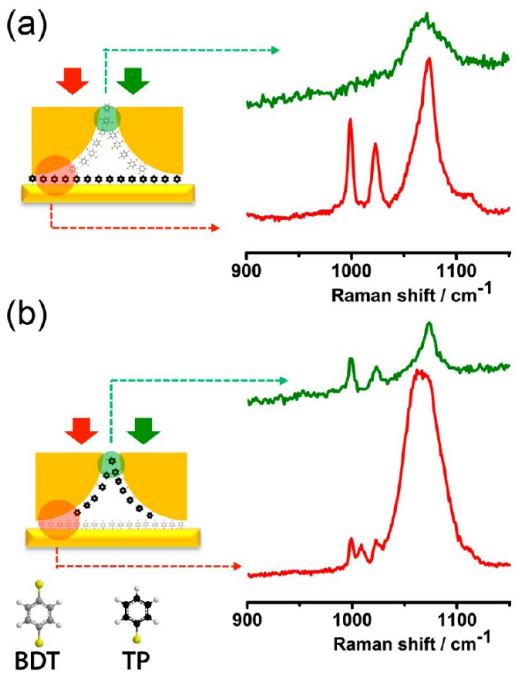

Figure 3. (a) Scheme for SERS detection with thiophenol (TP) molecules adsorbed in the gap between gold nanoparticles and the gold film and benzenedithiol (BDT) molecules adsorbed in the gap between nanoparticles. The green and red spectra were obtained with 532 and 633 nm excitation, respectively. (b) Similar to (a) with TP and BDT adsorbed at different locations.

The Raman spectrum (green line in Figure 3a) excited at 532 nm shows a broad peak at 1064 cm^{-1}, which comes from BDT molecules adsorbed at the gap between nanoparticles. Meanwhile, the peak at 998 cm^{-1} related to TP is absent. This is in good agreement with the previous simulation in Figure 1c where the hot spot totally locates at the gap between the gold nanoparticles. When we switched the excitation line to 633 nm, we obtained a spectrum (red line, Figure 3a) showing the intense characteristic peak of TP molecules at 998 cm^{-1}, which is located at the gap between the gold nanoparticles and the gold film. The experimental results agree very well with simulation and clearly demonstrate the feasibility of employing SERS to probe the near-field distribution of metal nanostructures. However, the peak at 1072 cm^{-1} (red line, Figure 3a) becomes broader than that of pure TP, as BDT molecules also contribute slightly to this peak. This phenomenon can be easily understood by the fact that BDT molecules can also be adsorbed to the curved edge outside the region of the nanoparticle–film gap, and they can also be enhanced, although slightly less, in the configuration of Figure 3a with red excitation.

To further verify our assumption, we changed the adsorption sequence to change the position of TP and BDT molecules. The configuration is shown in the left panel of Figure 3b, in which the TP molecules are adsorbed on nanoparticles and BDT molecules are adsorbed in the gap between nanoparticles and the gold film. We obtained a spectrum with signal mainly from TP excited at 532 nm, with the three sharp peaks appearing at 998, 1022, and 1072 cm^{-1}. When we changed the excitation line to 633 nm, we observed the strong signal from BDT with a broad peak at 1064 cm^{-1} and a weak signal from TP. This phenomenon can be also understood by the same reason as above, as TP molecules can also be adsorbed in the curved edge outside the gap between nanoparticles and the film; see Figure 3b. These experimental results are in very good agreement with the simulation result. To verify the influence of the molecules adsorbed in the curved edge of the gap, we designed another experiment, and the scheme and results are shown in the Supporting Information (S5). It demonstrated that the molecules adsorbed in the curved edge of the gap contribute little to the overall signals.

Both experimental and simulation results reveal that the location of the near-field enhancement will vary with the change of the excitation wavelengths for a specific metal nanostructure. Thus, one may obtain incorrect information without a proper understanding of SPR coupling modes and near-field distributions. It should be pointed out that, in the simulation above, we have a model of a nanoparticle dimer over a gold film. However in our experiment, we prepared a single layer of gold nanoparticles over a gold film. Therefore, one may wonder whether the presence of other nanoparticles will significantly change the coupling behavior as well as the near-field enhancement distribution of the system. The good agreement between the experiment and simulation result has indicated that this kind of effect may be negligible. But a proper theoretical understanding of the reason may have further important implications for experiment. In experiment, the nanoparticles are, in most cases, randomly dispersed on the substrate. How will the near-field distribution change with the variation of the number and the distribution of the nanoparticles and the distance between them?

For this purpose, we placed one more gold nanoparticle with a different distance to the gold nanoparticle dimer. The simulation was performed with 633 nm excitation, which is most commonly used for the gold nanoparticle system. The field distributions on the surface of the gold film are given in Figure 4. When a third gold nanoparticle was placed 1 nm from the dimer, the near-field distribution under the middle one spread to the nanoparticles at the two ends and presents a petal-like pattern (Figure 4b). This effect can be understood by the fact that the induced free

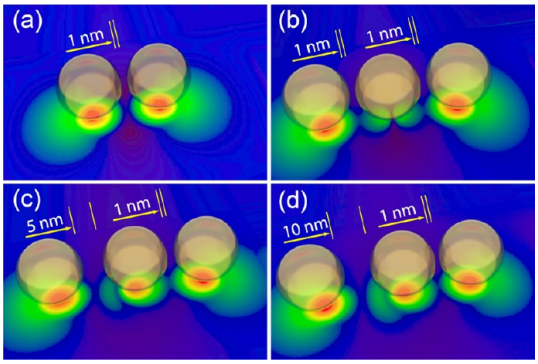

Figure 4. Images of the near-field distribution of the electric field on the upper surface of the gold film in the nanoparticles and gold−film coupling system simulated with FDTD. (a) Dimer with a separation of 1 nm. (b, c, d) Third gold nanoparticles placed 1, 5, and 10 nm away from the dimer in (a).

electrons in the gold film reservoir can be effectively coupled with the nanoparticles at the two ends with the polarization along the connecting axis of the nanoparticles. Thus few electrons are involved in the coupling with the middle one, leading to a weak near-field enhancement and a petal-like coupling pattern. In fact, this is a result of symmetry breaking induced by the presence of the third gold nanoparticle. If we further break the symmetry by placing the third nanoparticle at a larger distance, like 5 or 10 nm, the petal-like pattern disappears, as shown in Figure 4c and d. Although the near-field distribution on the gold film undergoes dramatic changes due to the presence of another nanoparticle or symmetry breaking, we did not see an obvious change in the enhancement factor in the near field. In fact, increasing the number of nanoparticles will increase the number of locations with a high near-field enhancement, which will eventually improve the efficiency for the SERS detection. In addition, the near-field enhancement between nanoparticles and the gold film is also independent of the aggregation of nanoparticles (Supporting Information S6).

The simulation result of multiple gold nanoparticles on the gold film reveals a promising feature of such a system: the enhancement on the metal surface is independent of the dispersing state of gold nanoparticles, which benefited from the fact that the 633 nm laser effectively excites only the coupling between nanoparticles and the gold film. This type of coupling depends on the distance between nanoparticles and the gold film, which is only controlled by the length of probe molecules (Figure 5a). In other word, we are able to achieve reproducible SERS detection by adsorbing probe molecules on a gold film first followed by dispersing with gold nanoparticles, which appears to be much easier than the traditional SERS substrates, which need to precisely control the distance between a large number of nanoparticles (Figure 5e). The parallel polarization for detecting molecules in the gap is compatible with the standard configuration of all the

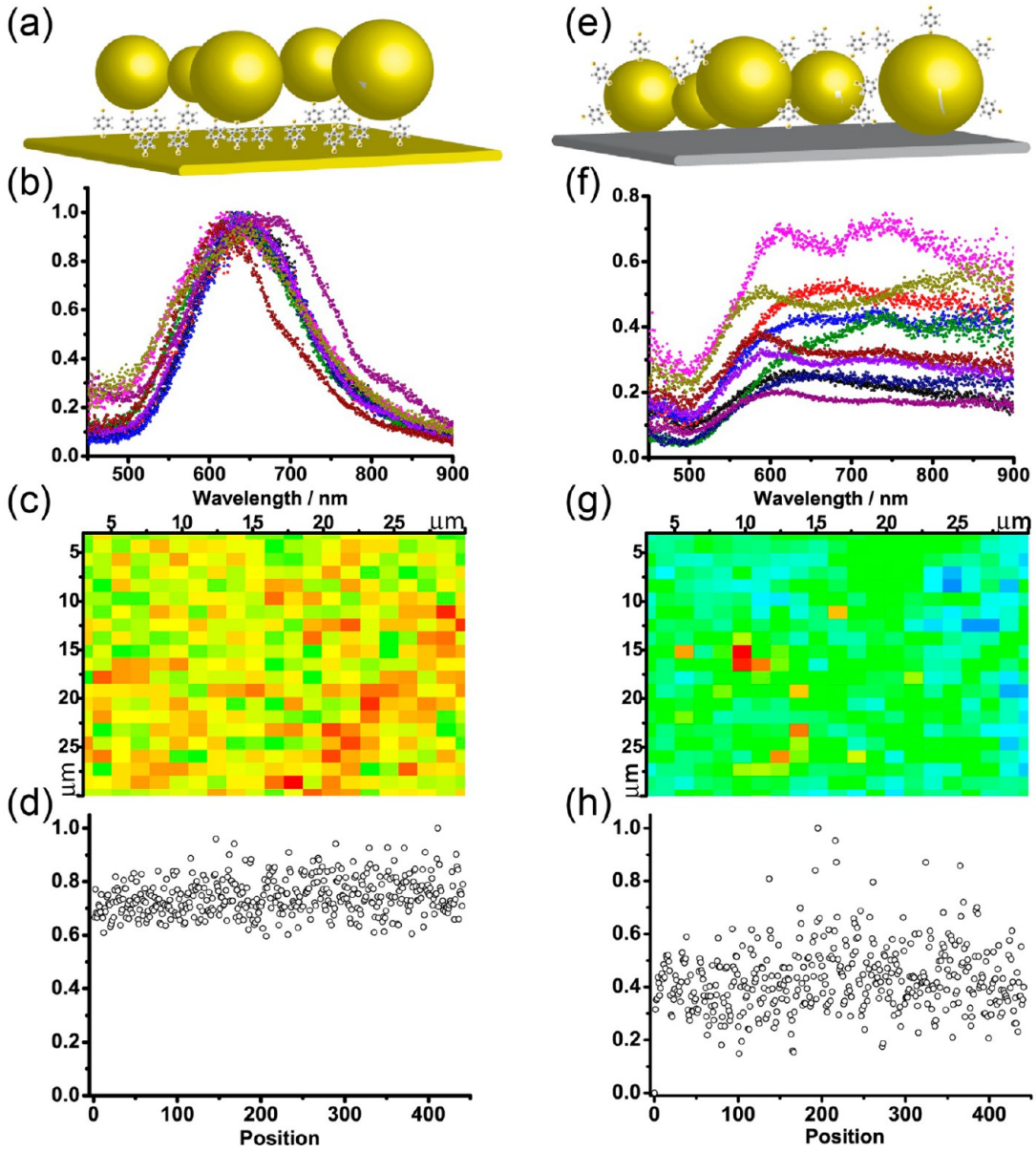

Figure 5. Comparison of the gap-mode SERS substrate (a−d) and the traditional SERS substrate (e−h). (a and e) Scheme for the two modes. (b and f) Scattering spectra obtained on the two substrates under a dark-field microscope. (c and g) Raman mapping images of the two substrates using the normalized intensity of the peak at 1064 cm^{-1}. The step size is 1.5 μm, and the mapping area is 30 $\times$ 30 μm^2. (d and h) Distribution of SERS intensity for the peak on the two substrates.

Raman instruments; that is, the excitation laser illuminates perpendicularly to the metal surface with its polarization parallel to the surface. Figure 5b and f show the scattering spectra of the gap-mode and traditional substrates, respectively. The gap-mode substrate presents a relatively narrow peak width, which can be understood by the identical distance between the nanoparticle and the film. However, the far-field scattering spectrum from experiment (Figure 5b) shows some deviation from the calculated one (Figure 1a). The discrepancy can be understood from the different response in the near field and far field. The electric-field enhancement (near field) between particles and the film is not affected by the distribution and aggregation states of particles, as shown in Figure 4 and Figure S7. Therefore the uniformity of SERS detection can be guaranteed. On the other hand, the scattering peaks (far field) are red-shifted with the increase of the distance between particles, as shown in Figure S8. Therefore, the experimentally obtained scattering spectra are the averaged spectra over all different distances, giving a wide peak around 600−700 nm. Up to now, it is still a great challenge to precisely control the distance between nanoparticles. The traditional substrate shows a much broader peak width over the visible region, because the SPR of this system is determined by the coupling between nanoparticles dispersed on the surface, and the unavoidable inhomogeneous

distribution of the nanoparticles on the surface leads to the broadening of the scattering band, as shown in Figure 5f.

We further evaluated the surface uniformity of SERS substrates by Raman mapping on the two types of substrates, and we measured two different substrates for each type to check the reproducibility. The mapping was performed over an area of 30 $\times$ 30 μm^2 with a 1.5 μm step and excited with a 633 nm laser. From the mapping result using the intensity of the peak (integrated peak area) at 1064 cm^{-1} for BDT molecules, we can easily see that the gap-mode type (Figure 5c) is more uniform than the traditional one (Figure 5g). Figure 5d and h plot the intensity of the peak over all the sampling points, and it is also clear that the variation is much smaller from the gap-mode SERS substrate than that from a traditional substrate. The relative standard deviations (RSD) of SERS intensity are about 9.3% and 10.9% for the two gap-mode SERS substrates. However, the RSD for the two traditional SERS substrates are 28.4% and 28.7%. Therefore, we can conclude that our gap-mode SERS substrate gives much more homogeneous signals, as we expected. This result can perfectly explain our previous work in SHINERS, in which we have achieved a very homogeneous response by simply dispersing SHINERS nanoparticles over a metallic single-crystal substrate preadsorbed with molecules.[24,25]

CONCLUSIONS

In conclusion, we have been able to precisely locate the position of different hot spots in a complex system of nanoparticles on a metal film with SERS by changing the excitation wavelengths and adsorbing different molecules (BDT or TP) at different surface sites. The feasibility to use SERS to probe the near-field distribution has important implications in surface plasmonics and surface analysis and also guides the design of metal nanostructures to improve the efficiency of SPR applications. The near-field enhancement corresponding to the coupling between nanoparticles and the coupling between nanoparticles and the gold film was found to be selectively excited with 532 and 633 nm lasers polarized parallel to the metal surface. The feasibility of a laser with the polarization perpendicular to the connecting axis of a coupling system seems to be against the notion of using the parallel polarization to excite a coupling system. The efficient excitation of SPR in the gap between gold nanoparticles and the gold film with a 633 nm laser offers us a unique opportunity to probe the information at the gap and the information for molecules adsorbed on the metal surface. The fact that the gap-mode SERS depends only on the distance between gold nanoparticles and the gold film (controlled by the length of probe molecules) provides a way to produce uniform SERS substrates: the probe molecule can be adsorbed on a metallic film first, followed by dispersing or adsorbing nanoparticles on the surface. This type of gap-mode SERS could provide the subtle chemical information on the surface with uniform signals over the substrate, which is important for surface analysis.

METHODS

Synthesis of Gold Nanoparticles. Gold nanoparticles were synthesized by a seed-mediated growth method. The seed of gold nanoparticles was synthesized according to Frens' method.[43] A 1.2 mL amount of 1% (weight/volume, w/v %) sodium citrate was added into 100 mL of boiled 0.01% (w/v %) chloroauric acid under strong stirring. The stirred solution was heated to reflux for 30 min to form the gold-nanoparticle seeds. After cooling, a 25 mL solution of gold-nanoparticle seeds was added into the mixture of 0.8 mL 1% sodium citrate and 50 mL of water. A 8.3 mL portion of 25 mM hydroxylamine was added 5 min later. Finally, 19 mL of 1 mM chloroauric acid was dropped into the solution slowly within 15 min. All the chemical agents were added under stirring and kept stirring for one more hour.

Fabrication of Gold-Nanoparticle Monolayer Films. The gold-nanoparticle monolayer film was fabricated according to Li's method.[44] A 5 mL amount of cyclohexane was added to a 50 mL beaker containing 15 mL of gold colloid. Then 4 mL of ethanol was dropped into the mixture. The gold nanoparticles were transferred from the aqueous solution to the interface between water and cyclohexane during the addition of ethanol. Afterward, most of the cyclohexane was removed with a syringe. A monolayer film of gold nanoparticles was formed due to the interfacial tension of the cyclohexane/water interface during the removal of cyclohexane. The gold-nanoparticle monolayer film can then be transferred to a solid support for further experiments.

Fabrication of Gold Nanoparticle–Film System with Adsorbed Molecules. The gold film with a thickness of 200 nm was fabricated by electron beam evaporation with Temescal FC2000 on glass slides. The root-mean-square roughness of the gold film was less than 0.5 nm, calculated from AFM data. Before use, the gold film was immersed in concentrated sulfuric acid for 15 min. Then it was rinsed by water and dried with nitrogen. A clean gold film was immersed in a 0.5 mM TP solution for 1 h and then rinsed with ethanol. After the TP-coated gold film was dry, a gold-nanoparticle monolayer film was transferred onto it. Thus the TP molecules were located at the gap between gold nanoparticles and the gold film. Then the substrate was again immersed in a 0.5 mM BDT solution for 1 h to let the BDT molecules adsorb on the nanoparticles. Thus we obtained the geometry shown in Figure 3a. The structure shown in Figure 3b was fabricated according to the following procedures. A clean gold film was immersed in a 0.5 mM BDT solution for 1 h and then rinsed with ethanol. After the BDT-coated gold film was dry, a gold-nanoparticle monolayer film was transferred onto it. Thus the BDT molecules were located at the gap between gold nanoparticles and the gold film. Then the substrate was again immersed in 0.5 mM TP solution for 1 h to let the TP molecules adsorb on nanoparticles.

Samples for Raman Mapping. The sample shown in Figure 5a was fabricated according to the following procedure. A gold film was immersed in a 0.5 mM ethanol solution of BDT for 1 h. Then it was rinsed by ethanol and dried with nitrogen. Finally the gold-nanoparticle monolayer film was transferred to the BDT-coated gold film. The sample shown in Figure 5e was fabricated according to the following procedure. The gold-nanoparticle monolayer film was transferred to a glass slide. Then the substrate was immersed in a 0.5 mM ethanol solution of BDT for 1 h. After that, it was rinsed by ethanol and dried with nitrogen.

Dark-Field Measurements. A Renishaw Raman instrument equipped with a Leica DM 2500 M dark-field microscope was

used to collect the scattering spectra of the substrates under dark-field illumination. We used a dark-field objective with 50× magnification, 0.55 NA, and a 150/mm grating. The background reference spectrum was collected at the place without nanoparticles. All the data shown in Figure 5b and f were corrected with background.

Raman Measurements. All the Raman detections in this paper were performed on a Renishaw inVia. The powers of the 633 and 532 nm laser on the sample were 0.21 and 0.15 mW, respectively, if they were not specified. We used a 50× objective with NA 0.55 and a 1800/mm grating. For Raman mapping, the mapping area was $30 \times 30\ \mu m^2$ with a step of 1.5 μm. The power of the 633 nm laser on the sample was 0.54 mW. The collection times for 532 nm and 633 nm are 60 s and 1 s, respectively.

Electrodynamic Simulations. The electromagnetic response of metal nanostructures was simulated by the FDTD method with a commercial software package (Lumerical Solutions, Inc. and Recom XFDTD). Scheme 1 shows the simulation model. It is composed of a gold nanoparticle dimer with a separation of 1 nm and placed 1 nm above a gold film. The gap size is close to the size of the molecule to achieve an effective coupling. The diameter of the gold nanoparticles is 55 nm, and the thickness of the gold film is 50 nm. The thickness has negligible effects on the optical response when the gold film is thicker than 50 nm (Supporting Information S8). The laser was illuminated perpendicularly to the metal surface following the experimental configuration, with the polarization parallel to the connecting axis of two gold particles and also parallel to the metal surface. The mesh unit was $1 \times 1 \times 1\ nm^3$. Different mesh units have been checked to ensure the credibility (Supporting Information S9). The dielectric constant of gold was from John and Christy.[45]

Conflict of Interest: The authors declare no competing financial interest.

Supporting Information Available: Simulation of a single gold nanoparticle on a gold film, SEM images of gold nanoparticles and the gold-nanoparticle monolayer film, comparison of SERS intensity of TP and BDT molecules, estimation of the contribution of the interstitial molecules adsorbed between the curved edge and the gold film to overall intensity, near-field distribution of aggregated nanoparticles excited at 633 nm, the influence of the distance between nanoparticles on the scattering spectra, the influence of thickness of the gold film on optical response, and simulation with different mesh units. This material is available free of charge *via* the Internet at http://pubs.acs.org.

Acknowledgment. Financial support from MOST (2011YQ03012406, 2013CB933703, and 2009CB930703) and NSFC (21021120456, 21321062, 21227004, J1310024, and 20825313) is highly acknowledged. We gratefully acknowledge the kind help from Christopher T. Williams in English writing and Bi-Ju Liu, Hai-Xin Lin, and Zhi-Chao Lei in Raman measurement and fabrication of gold nanoparticles.

REFERENCES AND NOTES

1. Anker, J. N.; Hall, W. P.; Lyandres, O.; Shah, N. C.; Zhao, J.; Van Duyne, R. P. Biosensing with Plasmonic Nanosensors. *Nat. Mater.* **2008**, *7*, 442–453.
2. Barnes, W. L.; Dereux, A.; Ebbesen, T. W. Surface Plasmon Subwavelength Optics. *Nature* **2003**, *424*, 824–830.
3. Gramotnev, D. K.; Bozhevolnyi, S. I. Plasmonics beyond the Diffraction Limit. *Nat. Photonics* **2010**, *4*, 83–91.
4. Schuller, J. A.; Barnard, E. S.; Cai, W. S; Jun, Y. C.; White, J. S.; Brongersma, M. I. Plasmonics for Extreme Light Concentration and Manipulation. *Nat. Mater.* **2010**, *9*, 193–204.
5. Jain, P. K.; Huang, X. H.; El-Sayed, I. H.; El-Sayed, M. A. Noble Metals on the Nanoscale: Optical and Photothermal Properties and Some Applications in Imaging, Sensing, Biology, and Medicine. *Acc. Chem. Res.* **2008**, *41*, 1578–1586.
6. Atwater, H. A.; Polman, A. Plasmonics for Improved Photovoltaic Devices. *Nat. Mater.* **2010**, *9*, 205–213.
7. Willets, K. A.; Van Duyne, R. P. Localized Surface Plasmon Resonance Spectroscopy and Sensing. *Annu. Rev. Phys. Chem.* **2007**, *58*, 267–297.
8. Anger, P.; Bharadwaj, P.; Novotny, L. Enhancement and Quenching of Single-Molecule Fluorescence. *Phys. Rev. Lett.* **2006**, *96*, 113002.
9. Chen, C. K.; de Castro, A. R. B.; Shen, Y. R. Surface-Enhanced Second-Harmonic Generation. *Phys. Rev. Lett.* **1981**, *46*, 145–148.
10. Moskovits, M. Surface-Enhanced Raman Spectroscopy: a Brief Retrospective. *J. Raman Spectrosc.* **2005**, *36*, 485–496.
11. Stiles, P. L.; Dieringer, J. A.; Shah, N. C.; Van Duyne, R. P. Surface-Enhanced Raman Spectroscopy. *Annu. Rev. Anal. Chem.* **2008**, *1*, 601–626.
12. Itoh, T.; Yoshida, K.; Biju, V.; Kikkawa, Y.; Ishikawa, M.; Ozaki, Y. Second Enhancement in Surface-Enhanced Resonance Raman Scattering Revealed by an Analysis of Anti-Stokes and Stokes Raman Spectra. *Phys. Rev. B.* **2007**, *76*, 085405.
13. Special Issue: Surface Enhanced Raman Spectroscopy. *J. Raman Spectrosc.* **2005**, *36*, 465−747.
14. Special Issue: Surface Enhanced Raman Spectroscopy. *Faraday Discuss.* **2006**, *132*, 1−320.
15. Thematic Issue: Surface Enhanced Raman Scattering. *Chem. Soc. Rev.* **2008**, *37*, 873−1076.
16. Themed Issue: New Frontiers in Surface Enhanced Raman Scattering. *Phys. Chem. Chem. Phys.* **2009**, *11*, 7333-7512.
17. Nie, S. M.; Emory, S. R. Probing Single Molecules and Single Nanoparticles by Surface-Enhanced Raman Scattering. *Science* **1997**, *275*, 1102–1106.
18. Kneipp, K.; Wang, Y.; Kneipp, H.; Perelman, L. T.; Itzkan, I.; Dasari, R. R.; Feld, S. Single Molecule Detection Using Surface-Enhanced Raman Scattering (SERS). *Phys. Rev. Lett.* **1997**, *78*, 1667–1670.
19. Xu, H. X.; Aizpurua, J.; Käll, M.; Apell, P. Electromagnetic Contributions to Single-Molecule Sensitivity in Surface-Enhanced Raman Scattering. *Phys. Rev. E* **2000**, *62*, 4318–4324.
20. Lin, X. M.; Cui, Y.; Xu, Y. H.; Ren, B.; Tian, Z. Q. Surface-Enhanced Raman Spectroscopy: Substrate-Related Issues. *Anal. Bioanal. Chem.* **2009**, *394*, 1729–1745.
21. Wang, H.; Levin, C. S.; Halas, N. J. Nanosphere Arrays with Controlled Sub-10-nm Gaps as Surface-Enhanced Raman Spectroscopy Substrates. *J. Am. Chem. Soc.* **2005**, *127*, 14992–14993.
22. Mahajan, S.; Baumberg, J. J.; Russell, A. E.; Bartlett, P. N. Reproducible SERRS from Structured Gold Surfaces. *Phys. Chem. Chem. Phys.* **2007**, *9*, 6016–6020.
23. Knight, M. W.; Wu, Y. P.; Lassiter, J. B.; Nordlander, P.; Halas, N. J. Substrates Matter: Influence of an Adjacent Dielectric on an Individual Plasmonic Nanoparticle. *Nano Lett.* **2009**, *9*, 2188–2192.
24. Li, J. F.; Huang, Y. F.; Ding, Y.; Yang, Z. L.; Li, S. B.; Zhou, X. S.; Fan, F. R.; Zhang, W.; Zhou, Z. Y.; Wu, D. Y.; *et al.* Shell-Isolated Nanoparticle-Enhanced Raman Spectroscopy. *Nature* **2010**, *464*, 392–395.
25. Li, J. F.; Ding, S. Y.; Yang, Z. L.; Bai, M. L.; Anema, J. R.; Wang, X.; Wang, A.; Wu, D. Y.; Ren, B.; Hou, S. M. Extraordinary Enhancement of Raman Scattering from Pyridine on Single Crystal Au and Pt Electrodes by Shell-Isolated Au Nanoparticles. *J. Am. Chem. Soc.* **2011**, *133*, 15922–15925.
26. Huang, Y. F.; Yin, N. N.; Wang, X.; Wu, D. Y.; Ren, B.; Tian, Z. Q. Vibrational Signature of Double-End-Linked Molecules at Au Nanojunctions Probed by Surface-Enhanced Raman Spectroscopy. *Chem.—Eur. J.* **2010**, *16*, 1449–1453.
27. Fang, Y.; Huang, Y. Electromagnetic Field Redistribution in Hybridized Plasmonic Particle-Film System. *Appl. Phys. Lett.* **2013**, *102*, 153108.
28. Xu, H. X.; Bjerneld, E. J.; Käll, M.; Börjesson, L. Spectroscopy of Single Hemoglobin Molecules by Surface Enhanced Raman Scattering. *Phys. Rev. Lett.* **1999**, *83*, 4357–4360.
29. Hao, E.; Schatz, G. C. Electromagnetic Fields around Silver Nanoparticles and Dimers. *J. Chem. Phys.* **2004**, *120*, 357–366.
30. Kim, K.; Shin, D.; Kim, K. L.; Shin, K. S. Electromagnetic Field Enhancement in the Gap between Two Au Nanoparticles: the Size of Hot Site Probed by Surface-Enhanced Raman Scattering. *Phys. Chem. Chem. Phys.* **2010**, *12*, 3747–3752.

31. Nordlander, P.; Le, F. Plasmonic Structure and Electromagnetic Field Enhancements in the Metallic Nanoparticle-Film System. *Appl. Phys. B: Laser Opt.* **2006**, *84*, 35–41.
32. Le, F.; Lwin, N. Z.; Halas, N. J.; Nordlander, P. Plasmonic Interactions between a Metallic Nanoshell and a Thin Metallic Film. *Phys. Rev. B* **2007**, *76*, 165410.
33. Park, W. H.; Ahn, S. H.; Kim, Z. H. Surface-Enhanced Raman Scattering from a Single Nanoparticle−Plane Junction. *ChemPhysChem* **2008**, *9*, 2491–2494.
34. Lei, D. Y.; Fernández-Domínguez, A. I.; Sonnefraud, Y.; Appavoo, K.; Haglund, R. F.; Pendry, J. B.; Maier, S. A. Revealing Plasmonic Gap Modes in Particle-on-Film Systems Using Dark-Field Spectroscopy. *ACS Nano* **2012**, *6*, 1380–1386.
35. Ikeda, K.; Fujimoto, N.; Uehara, H.; Uosaki, K. Raman Scattering of Aryl Isocyanide Monolayers on Atomically Flat Au(111) Single Crystal Surfaces Enhanced by Gap-Mode Plasmon Excitation. *Chem. Phys. Lett.* **2008**, *460*, 205–208.
36. Hecht, B.; Sick, B.; Wild, U. P.; Deckert, V.; Zenobi, R.; Martin, O. J. F.; Pohl, D. W. Scanning Near-Field Optical Microscopy with Aperture Probes: Fundamentals and Applications. *J. Chem. Phys.* **2000**, *112*, 7761–7774.
37. Ringe, E.; Sharma, B.; Henry, A. I.; Marks, L. D.; Van Duyne, R. P. Single Nanoparticle Plasmonics. *Phys. Chem. Chem. Phys.* **2013**, *15*, 4110–4129.
38. Le Ru, E. C.; Etchegoin, P. G.; Meyer, M. Enhancement Factor Distribution around a Single Surface-Enhanced Raman Scattering Hot Spot and Its Relation to Single Molecule Detection. *J. Chem. Phys.* **2006**, *125*, 204701.
39. Le Ru, E. C.; Etchegoin, P. G. Single-Molecule Surface-Enhanced Raman Spectroscopy. *Annu. Rev. Phys. Chem.* **2012**, *63*, 65–87.
40. Fang, Y.; Seong, N. H.; Dlott, D. D. Measurement of the Distribution of Site Enhancements in Surface-Enhanced Raman Scattering. *Science* **2008**, *321*, 388–392.
41. Weber, M. L.; Willets, K. A. Correlated Super-Resolution Optical and Structural Studies of Surface-Enhanced Raman Scattering Hot Spots in Silver Colloid Aggregates. *J. Phys. Chem. Lett.* **2011**, *2*, 1766–1770.
42. Willets, K. A.; Stranahan, S. M.; Weber, M. L. Shedding Light on Surface-Enhanced Raman Scattering Hot Spots through Single-Molecule Super-Resolution Imaging. *J. Phys. Chem. Lett.* **2012**, *3*, 1286–1294.
43. Frens, G. Controlled Nucleation for the Regulation of the Particle Size in Monodisperse Gold Suspensions. *Nat. Phys. Sci.* **1973**, *241*, 20–22.
44. Li, Y. J.; Huang, W. J.; Sun, S. G. A Universal Approach for the Self-Assembly of Hydrophilic Nanoparticles into Ordered Monolayer Films at a Toluene/Water Interface. *Angew. Chem., Int. Ed.* **2006**, *45*, 2537–2539.
45. Johnson, P. B.; Christy, R. W. Optical Constants of the Noble Metals. *Phys. Rev. B* **1972**, *6*, 4370–4379.